Acta Astronautica 139 (2017) 201–212

Contents lists available at ScienceDirect

Acta Astronautica

journal homepage: www.elsevier.com/locate/actaastro

Drift-free solar sail formations in elliptical Sun-synchronous orbits

Khashayar Parsay *, Hanspeter Schaub

Aerospace Engineering Sciences Department, 431 UCB, Colorado Center for Astrodynamics Research, University of Colorado, Boulder, CO, 80309-0431, USA

ARTICLE INFO

Keywords:
Solar sail
Formation flying
Magnetosphere mission

ABSTRACT

To study the spatial and temporal variations of plasma in the highly dynamic environment of the magnetosphere, multiple spacecraft must fly in a formation. The objective for this study is to investigate the feasibility of solar sail formation flying in the Earth-centered, Sun-synchronous orbit regime. The focus of this effort is to enable formation flying for a group of solar sails that maintain a nominally *fixed* Sun-pointing attitude during formation flight, solely for the purpose of precessing their orbit apse lines Sun-synchronously. A fixed-attitude solar sail formation is motivated by the difficulties in the simultaneous control of orbit and attitude in flying solar sails. First, the secular rates of the orbital elements resulting from the effects of solar radiation pressure (SRP) are determined using averaging theory for a Sun-pointing attitude sail. These averaged rates are used to analytically derive the first-order necessary conditions for a drift-free solar sail formation in Sun-synchronous orbits, assuming a fixed Sun-pointing orientation for each sail in formation. The validity of the first-order necessary conditions are illustrated by designing quasi-periodic relative motions. Next, nonlinear programming is applied to design truly drift-free two-craft solar sail formations. Lastly, analytic expressions are derived to determine the long-term dynamics and sensitivity of the formation with respect to constant attitude errors, uncertainty in orbital elements, and uncertainty in a sail's characteristic acceleration.

1. Introduction

The Earth's magnetic field is continuously subjected to strong interactions with charged particles, leading to many complicated phenomena such as magnetic reconnection. Magnetic reconnection is a poorly understood phenomenon that occurs when magnetic field lines realign and magnetic energy is converted to thermal and kinetic energy [1].

Most of what is known about magnetic reconnection comes from theoretical studies and computer models. Laboratory experiments on magnetic reconnection have been carried out, such as the Magnetic Reconnection Experiment (MRX) at Princeton Plasma Physics Laboratory (PPPL). But despite five decades of research, magnetic reconnection and its overall operation remain poorly understood. Learning about magnetic reconnection will allow for the prediction of this universal process which affects our technological systems, including communications networks, GPS navigation, and electrical power grids. The key to understanding this physical process lies in the particle measurements of reconnection sites via in situ observation. The reconnection sites are initially very small, between 1000–10,000 km, and vary with solar activity. Furthermore, reconnections last at most a few minutes per substorm occurrence, which can happen once per three hours. For these reasons, in situ observation of magnetic reconnection is a challenging task [1,2]. Achieving long residence times in the geomagnetic tail is therefore particularly important for studying the magnetic reconnection phenomena.

The Earth's magnetic tail is directed along the Sun-Earth line and therefore rotates annually. Conventional magnetosphere missions require a highly elliptical orbit with its apogee inside the geomagnetic tail. The placement of the orbit apogee within a specific region of interest allows for the maximization of time the spacecraft spends in that region. An inertially fixed orbit is aligned with the geomagnetic tail only once a year, which limits the continuous presence and duration of the science phase to less than three months. Solar sail low-thrust propulsion, however, is capable of achieving long residence times in the geomagnetic tail by continuously precessing the orbit apse line, as illustrated in Fig. 1.

McInnes and Macdonald propose the novel low-cost GEOSAIL mission to explore the Earth's magnetosphere using a single low performance sail [3–5]. In the GEOSAIL mission, the approximately 2000 m^2 solar sail would fly in a moderately elliptical orbit of size 10 R_E × 30 R_E that lies in the ecliptic plane and would employ a simple Sun-pointing steering law to precess the orbit apse line Sun-synchronously, allowing the orbit apogee to remain in the geomagnetic tail throughout the entire year. This

* Corresponding author.
E-mail addresses: khashayar.parsay@colorado.edu (K. Parsay), hanspeter.schaub@colorado.edu (H. Schaub).

http://dx.doi.org/10.1016/j.actaastro.2017.06.027
Received 23 November 2016; Received in revised form 24 April 2017; Accepted 27 June 2017
Available online 1 July 2017

Nomenclature

$\boldsymbol{r}$	Sail position vector [km]
μ	Earth's gravitational constant [km^3/s^2]
$\boldsymbol{a}_s$	Solar radiation pressure acceleration [km/s^2]
$\boldsymbol{a}_\oplus$	Acceleration due to Earth's nonsphericity [km/s^2]
$\boldsymbol{a}_\leftmoon$	Acceleration due to moon's gravity [km/s^2]
$\boldsymbol{a}_\odot$	Acceleration due to sun's gravity [km/s^2]
$\hat{\boldsymbol{n}}_s$	Sun-line unit vector
$\hat{\boldsymbol{n}}$	Sail normal unit vector
a_r, a_θ, a_h	Solar radiation pressure acceleration along radial, along-track, and cross-track direction [km/s^2]
$\boldsymbol{\alpha}$	Array containing classical orbital elements $[a, e, i, \Omega, \omega, f]^T$. a: semi-major axis [km], e: eccentricity, i: inclination [rad], Ω: right ascension of ascending node [rad], ω: argument of perigee [rad], f: true anomaly [rad]
T	Orbit period [s]
k	Characteristic acceleration of solar sail [km/s^2]
$[\boldsymbol{C}_i]$	Rotation matrix about the i axis
$\mathscr{O}$	Local-vertical-local-horizontal (LVLH) frame
$\mathscr{N}$	Earth-centered inertial frame
$[\mathscr{N}\mathscr{O}]$	Direction cosine matrix that transfers a vector from $\mathscr{O}$ to $\mathscr{N}$ frame in chief's LVLH frame
λ_s	Sun longitude measured from vernal equinox [rad]
c	Denotes the chief solar sail
d	Denotes the deputy solar sail

Acronym

SRP	Solar radiation pressure
R_E	Earth radius

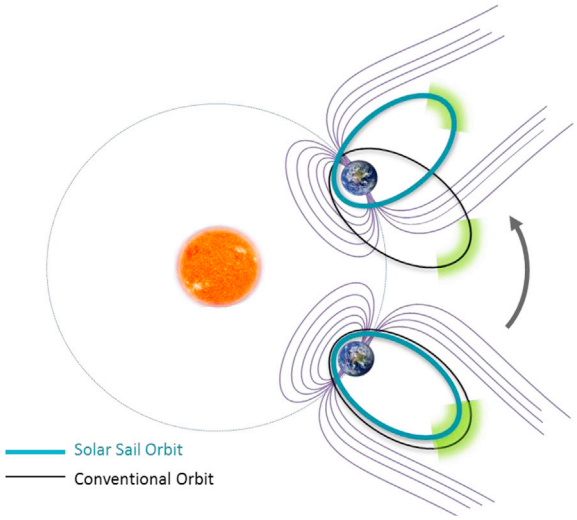

Fig. 1. Comparison of chemical and solar sail propulsion in geomagnetic tail exploration.

particular orbit belongs to a general class of orbits discussed by Rosengren and Scheeres in Ref. [14], where an explicit closed-form solution for the motion of an object orbiting a planet subjected to SRP acceleration is derived analytically, using Milankovitch orbital elements. Note that in this paper, when an orbit is referred to as Sun-synchronous, it should not be confused with a conventional Sun-synchronous orbit whose precession rate of longitude of ascending node equals the mean motion of the Earth about the Sun.

Many magnetosphere missions require more than a single spacecraft to achieve their scientific objective. Gong and Mu propose solar sail formation flying for exploring the geomagnetic tail [6–10]. These studies propose *steered* formation flying, where the deputy sails must continuously change their orientations to maintain a desired unnatural relative motion with respect to the chief solar sail, who employs a Sun-pointing attitude to remain in a Sun-synchronous orbit.

Similar to Ref. [11], this paper takes a completely different approach, namely natural formation flying, where all solar sails in formation maintain a *fixed* or *unsteered* Sun-pointing attitude solely for the purpose of precessing their orbit apse lines Sun-synchronously. This work, however, significantly improves upon the work in Ref. [11] by deriving the general first-order necessary conditions for SRP invariant relative orbits. These conditions lead to finding truely SRP invariant relative orbits, as opposed to quasi-periodic relative orbits that experience a non-negligible drift rate.

This paper is organized as follows. Section 2 reviews how a solar sail may be used to artificially precess the orbit apse line Sun-synchronously [3,4]. In Section 3, averaging theory is used to determine the secular variations in the orbital elements due to the SRP force resulting from Sun-pointing attitude. In Section 4, the necessary conditions for achieving SRP invariant solar sail formation flight in Sun-synchronous orbits are derived. In Section 5, it is illustrated how the first-order necessary conditions lead to quasi-periodic relative motions that experience some relative drift due to truncation of the higher order terms. In Section 6, numerical optimization techniques are employed to remove any relative drift arising from the first-order approximation. Employing numerical methods leads to the design of truly SRP invariant relative motions in Sun-synchronous orbits. In Section 7, averaging theory is applied to determine the sensitivity of the formation with respect to constant attitude errors. A set of elegant analytic expressions for the orbital element rates is derived that accurately predicts the long terms effects of uncertainty in the sail's attitude on the orbital elements. The effects of uncertainty in orbital elements and uncertainty in sail's characteristic acceleration are explored in Section 8.

2. Equations of motion of solar sails in earth orbits

The general equations of motion for a solar sail in an Earth orbit is written as

$$\ddot{\boldsymbol{r}} = -\frac{\mu}{r^3}\boldsymbol{r} + \boldsymbol{a}_\oplus + \boldsymbol{a}_\leftmoon + \boldsymbol{a}_\odot + \boldsymbol{a}_s \tag{1}$$

where $\boldsymbol{r}$ is the position vector of the spacecraft relative to the Earth and $\boldsymbol{a}_\oplus$, $\boldsymbol{a}_\leftmoon$, $\boldsymbol{a}_\odot$, and $\boldsymbol{a}_s$ are the accelerations due to Earth's nonsphericity, lunar gravitational effects, solar gravitational effects, and solar radiation pressure respectively. The adopted inertial frame $\mathscr{N} = \{O, \boldsymbol{X}, \boldsymbol{Y}, \boldsymbol{Z}\}$ has its origin O at the center of the Earth where the $\boldsymbol{X}$ axis points from the origin to the equinox and $\boldsymbol{Z}$ points along the ecliptic north pole. The $\boldsymbol{Y}$ axis completes the right-handed coordinate system. For a flat, rigid, perfectly reflecting solar sail, the solar sail's acceleration due to the SRP can be written as

$$\boldsymbol{a}_s = k(\hat{\boldsymbol{n}}_s \cdot \hat{\boldsymbol{n}})^2 \hat{\boldsymbol{n}} \tag{2}$$

where $\hat{\boldsymbol{n}}$ is a unit vector normal to the sail surface, $\hat{\boldsymbol{n}}_s$ is the Sun unit vector, and the parameter k is the sail's characteristic acceleration, which is defined as the acceleration experienced by the solar sail at a heliocentric distance of 1 astronomical unit (AU) while the sail normal is directed along the sun-line [12]. For the GEOSAIL mission, McInnes and Macdonald propose flying a solar sail in the ecliptic plane using a simple steering law consisting of the sail's normal vector continuously pointing

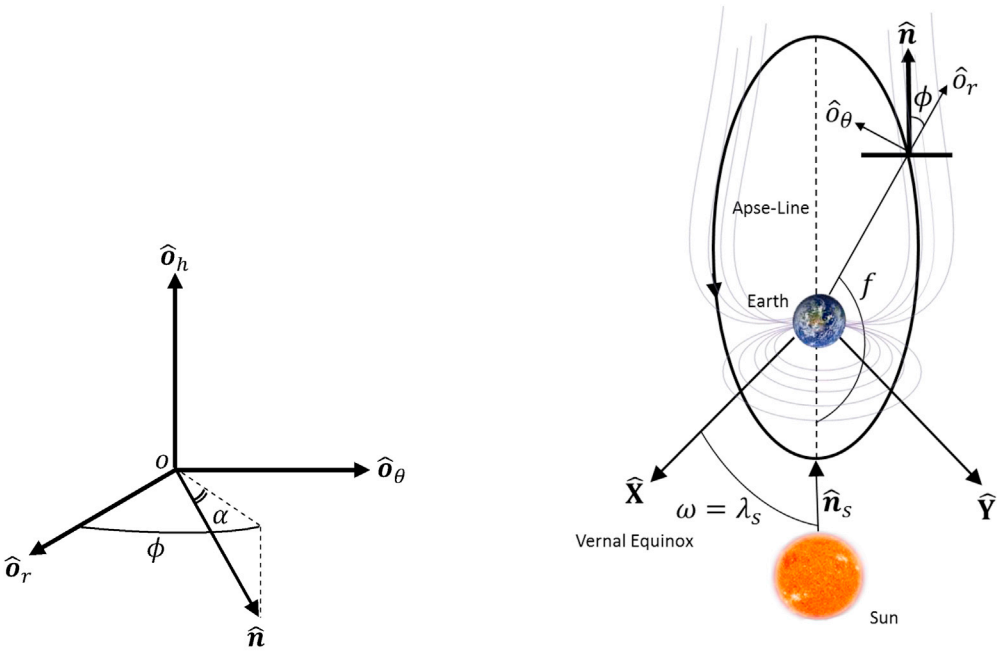

(a) Sail's normal vector orientation in the LVLH frame (b) Solar sail geometry in Sun-synchronous orbit

Fig. 2. Sail's orbit geometry and general orientation.

along the Sun-line within the orbit plane such that the rotation of the orbit apse-line is synchronous with the annual rotation of the Sun-line [3–5]. The Sun-synchronized precession of the orbit apse-line allows the orbit apogee to remain in the geomagnetic tail continuously, thus enabling science data collection for long periods. The required characteristic acceleration k to precess the orbit Sun-synchronously is dependent on the shape of the orbit and is computed according to [3,4]

$$k(a,e) = \frac{2}{3}\dot{\lambda}_s \frac{e}{\sqrt{1-e^2}}\sqrt{\frac{\mu}{a}} \tag{3}$$

To describe the $\hat{\boldsymbol{n}}$ vector resulting from the Sun-pointing steering law in the inertial frame $\mathcal{N}$, a local reference frame must be defined. Let $\mathcal{O} = \{o,\ \hat{\boldsymbol{o}}_r,\ \hat{\boldsymbol{o}}_\theta,\ \hat{\boldsymbol{o}}_h\}$ define the sail's local-vertical-local-horizontal (LVLH) reference frame with its origin point o at the sail's center of mass, where $\hat{\boldsymbol{o}}_r$ points along the sail's position vector, $\hat{\boldsymbol{o}}_h$ is directed along the orbit angular momentum vector, and $\hat{\boldsymbol{o}}_\theta = \hat{\boldsymbol{o}}_h \times \hat{\boldsymbol{o}}_r$ completes the right-handed coordinate system. As shown in Fig. 2(a), the α and ϕ angles track the orientation of the sail's normal with respect to the $\mathcal{O}$ frame. Thus, the sail's normal vector is expressed in the $\mathcal{O}$ frame as

$${}^{\mathcal{O}}\hat{\boldsymbol{n}} = {}^{\mathcal{O}}\begin{bmatrix} \cos\alpha\cos\phi \\ \cos\alpha\sin\phi \\ -\sin\alpha \end{bmatrix} \tag{4}$$

where the left-superscript indicates the frame that the $\hat{\boldsymbol{n}}$ vector is expressed in. As illustrated in Fig. 2(b), the sail's normal $\hat{\boldsymbol{n}}$ points along the Sun-line within the ecliptic plane such that the identity $\omega = \lambda_s$ and $\hat{\boldsymbol{n}}\cdot\hat{\boldsymbol{n}}_s = 1$ hold. This leads to orbit apse-line always pointing along the sun-line $\hat{\boldsymbol{n}}_s$. The SRP acceleration $\boldsymbol{a}_s$ expressed in the LVLH frame may be written as

$${}^{\mathcal{O}}\boldsymbol{a}_s = k(\hat{\boldsymbol{n}}_s\cdot\hat{\boldsymbol{n}})^2\,{}^{\mathcal{O}}\hat{\boldsymbol{n}} = {}^{\mathcal{O}}\begin{bmatrix} a_r \\ a_\theta \\ a_h \end{bmatrix} = {}^{\mathcal{O}}\begin{bmatrix} k\cos\alpha\cos\phi \\ k\cos\alpha\sin\phi \\ -k\sin\alpha \end{bmatrix}$$

The sail's assumed orientation results in having $\phi = \pi - f$ and $\alpha = 0$. Substituting these identities to Eq. (4), the sail's normal vector may be further simplified to

$${}^{\mathcal{O}}\hat{\boldsymbol{n}} = {}^{\mathcal{O}}\begin{bmatrix} -\cos f \\ \sin f \\ 0 \end{bmatrix} \tag{5}$$

The direction cosine matrix $[\mathcal{N}\mathcal{O}] = [{}^{\mathcal{N}}\hat{\boldsymbol{o}}_r\ {}^{\mathcal{N}}\hat{\boldsymbol{o}}_\theta\ {}^{\mathcal{N}}\hat{\boldsymbol{o}}_h]$ is used to transfer the sail's normal ${}^{\mathcal{O}}\hat{\boldsymbol{n}}$ from the reference frame $\mathcal{O}$ to the inertial frame $\mathcal{N}$ to be used in Eq. (1). Thus the sail's normal expressed in the $\mathcal{N}$ frame is

$${}^{\mathcal{N}}\hat{\boldsymbol{n}} = [\mathcal{N}\mathcal{O}]\,{}^{\mathcal{O}}\hat{\boldsymbol{n}} \tag{6}$$

The sunlight direction expressed in the inertial frame $\mathcal{N}$ can be written as

$${}^{\mathcal{N}}\hat{\boldsymbol{n}}_s = {}^{\mathcal{N}}\begin{bmatrix} -\cos\lambda_s \\ -\sin\lambda_s \\ 0 \end{bmatrix} \tag{7}$$

where the longitude of the Sun λ_s is determined through

$$\lambda_s = \lambda_{s_0} + \dot{\lambda}_s t \tag{8}$$

Finally, the SRP acceleration ${}^{\mathcal{N}}\boldsymbol{a}_s$ is determined by substituting Eq. (6) and Eq. (7) into Eq. (2). The mission orbit considered in this paper is a 11 R_E × 30 R_E orbit that lies in the ecliptic plane. The corresponding orbit period is $T = 5.4457$ days. The orbital elements for the mission orbit are $a = 130751.8$ km, $e = 0.4634$, $i = 0$ deg, $\omega = 0$ deg, and $\Omega = 0$ deg.

3. Average effects of SRP in Sun-synchronous orbits

In this section, averaging theory is used to determine the secular variations in the orbital elements due to the SRP perturbing force in Sun-synchronous orbits. Classical averaging theory was mainly developed in order to study nonlinear non-autonomous systems and it's a powerful tool in determining the long-term dynamics of artificial and natural satellites in orbital mechanics [13–18]. The Gauss Variational equations are given as follows [19]

$$\dot{a} = \frac{2a^2}{h}\left(e\sin f a_r + \frac{p}{r}a_\theta\right) \tag{9a}$$

$$\dot{e} = \frac{1}{h}(p \sin f a_r + [(p+r)\cos f + re]a_\theta) \tag{9b}$$

$$\dot{i} = \frac{r\cos\theta}{h} a_h \tag{9c}$$

$$\dot{\Omega} = \frac{r\sin\theta}{h\sin i} a_h \tag{9d}$$

$$\dot{\omega} = \frac{1}{he}(-p\cos f a_r + (p+r)\sin f a_\theta) \tag{9e}$$

$$\dot{M} = n + \frac{b}{ahe}((p\cos f - 2re)a_r - (p+r)\sin f a_\theta) \tag{9f}$$

After substituting the SRP perturbing acceleration in Eq. (2) into Eq. (9), we have

$$\dot{a} = \frac{2a^2 k \sin f}{\sqrt{a(1-e^2)\mu}} \tag{10a}$$

$$\dot{e} = \frac{k\sqrt{a(1-e^2)\mu}(e+\cos f)\sin f}{\mu(1+e\cos f)} \tag{10b}$$

$$\dot{\omega} = \frac{k\sqrt{a(1-e^2)\mu}(2e\cos f - \cos 2f + 3)}{2e\mu(1+e\cos f)} \tag{10c}$$

$$\dot{M} = n + \frac{k(a^2(1-e^2))^{3/2}(2e\cos f + \cos 2f - 3)}{2a^2 e\sqrt{a(1-e^2)\mu}(e\cos f + 1)} \tag{10d}$$

Note the appearance of the true anomaly variable f in all terms. To remove the short-term variations and extract the secular variations, we average each element separately as follows [13],

$$\dot{\bar{a}} = \frac{1}{2\pi}\int_0^{2\pi} \dot{a}\, \mathrm{d}M = \frac{1}{2\pi}\int_0^{2\pi} \gamma \dot{a} \mathrm{d}f \tag{11a}$$

$$\dot{\bar{e}} = \frac{1}{2\pi}\int_0^{2\pi} \dot{e}\, \mathrm{d}M = \frac{1}{2\pi}\int_0^{2\pi} \gamma \dot{e} \mathrm{d}f \tag{11b}$$

$$\dot{\bar{\omega}} = \frac{1}{2\pi}\int_0^{2\pi} \dot{\omega}\, \mathrm{d}M = \frac{1}{2\pi}\int_0^{2\pi} \gamma \dot{\omega} \mathrm{d}f \tag{11c}$$

$$\dot{\bar{M}} = \frac{1}{2\pi}\int_0^{2\pi} \dot{M}\, \mathrm{d}M = \frac{1}{2\pi}\int_0^{2\pi} \gamma \dot{M} \mathrm{d}f \tag{11d}$$

The averaging must be performed with respect to the mean anomaly variable M. Because the equations in Eq. (10) are all expressed in terms of true anomaly, a change of variable is required before performing the integration. This change of variable is given by,

$$\mathrm{d}M = \frac{n}{h} r^2 \mathrm{d}f = \gamma\, \mathrm{d}f \tag{12}$$

Performing the integration, the secular variations of orbital elements due to the SRP force are written as,

$$\dot{\bar{a}} = 0 \tag{13a}$$

$$\dot{\bar{e}} = 0 \tag{13b}$$

$$\dot{\bar{\omega}} = \frac{3k\sqrt{\bar{a}(1-\bar{e}^2)}}{2\bar{e}\sqrt{\mu}} \tag{13c}$$

$$\dot{\bar{M}} = \bar{n} - \frac{3\sqrt{\bar{a}}(1+\bar{e}^2)k}{2\bar{e}\sqrt{\mu}} \tag{13d}$$

Note that if the characteristic acceleration is governed by Eq. (3), then Eq. (13) simplifies to the following expressions,

$$\dot{\bar{a}} = 0 \tag{14a}$$

$$\dot{\bar{e}} = 0 \tag{14b}$$

$$\dot{\bar{\omega}} = \dot{\lambda}_s \tag{14c}$$

$$\dot{\bar{M}} = \bar{n} - \frac{1+\bar{e}^2}{\sqrt{1-\bar{e}^2}}\dot{\lambda}_s \tag{14d}$$

The average value of $\dot{a}$ is zero which is a classical result; the semi-major axis experiences no secular change as a result of SRP perturbation. It turns out that the eccentricity experiences no secular variation for a solar sail in a Sun-synchronous orbit. The only two elements that experience secular variations are the argument of perigee ω and the mean anomaly M. Note that if $k = 0$ (no reflectivity), we would have $\dot{\bar{\omega}} = 0$, and $\dot{\bar{M}} = n$, which are the classical results from the two-body problem. The results in Eq. (13) are critical for determining the necessary conditions to fly a drift-free solar sail formation in a Sun-synchronous orbit. The next section details how Eq. (13) may be used to derive first-order necessary conditions for SRP invariant relative motion in Sun-synchronous orbits.

4. Necessary conditions for SRP invariant relative motion

For the relative motion of two solar sails in Sun-synchronous orbits to remain invariant to the relative effects of SRP, the following two secular drift rates must be matched,

$$\dot{\bar{\omega}}_d = \dot{\bar{\omega}}_c \tag{15a}$$

$$\dot{\bar{M}}_d = \dot{\bar{M}}_c \tag{15b}$$

Assuming that two solar sails are flying in close-proximity and have a negligible difference between their characteristic accelerations, the first-order approximation of the deputy's average rates can be written in terms of the chief's average rates using,

$$\dot{\bar{\omega}}_d = \dot{\bar{\omega}}_c(\bar{a}_c, \bar{e}_c, k_c) + \delta\dot{\bar{\omega}} = \dot{\bar{\omega}}_c \tag{16a}$$

$$+\frac{\partial\dot{\bar{\omega}}}{\partial\bar{a}}\Big|_{\bar{a}_c,\bar{e}_c,k_c}\delta\bar{a} + \frac{\partial\dot{\bar{\omega}}}{\partial\bar{e}}\Big|_{\bar{a}_c,\bar{e}_c,k_c}\delta\bar{e} + \frac{\partial\dot{\bar{\omega}}}{\partial k}\Big|_{\bar{a}_c,\bar{e}_c,k_c}\delta k \tag{16b}$$

$$\dot{\bar{M}}_d = \dot{\bar{M}}_c(\bar{a}_c, \bar{e}_c, k_c) + \delta\dot{\bar{M}} = \dot{\bar{M}}_c \tag{16c}$$

$$+\frac{\partial\dot{\bar{M}}}{\partial\bar{a}}\Big|_{\bar{a}_c,\bar{e}_c,k_c}\delta\bar{a} + \frac{\partial\dot{\bar{M}}}{\partial\bar{e}}\Big|_{\bar{a}_c,\bar{e}_c,k_c}\delta\bar{e} + \frac{\partial\dot{\bar{M}}}{\partial k}\Big|_{\bar{a}_c,\bar{e}_c,k_c}\delta k \tag{16d}$$

where the partials are all evaluated with respect to the chief's orbital elements and can be expressed using,

$$\frac{\partial\dot{\bar{\omega}}}{\partial\bar{a}}\Big|_{\bar{a},\bar{e},k} = \frac{3(1-\bar{e}^2)k}{4\bar{e}\sqrt{\bar{a}(1-\bar{e}^2)\mu}} \tag{17a}$$

$$\frac{\partial\dot{\bar{\omega}}}{\partial\bar{e}}\Big|_{\bar{a},\bar{e},k} = -\frac{3\bar{a}k}{2\bar{e}^2\sqrt{\bar{a}(1-\bar{e}^2)\mu}} \tag{17b}$$

$$\frac{\partial \dot{\bar{\omega}}}{\partial k}\Big|_{\bar{a},\bar{e},k} = \frac{3\sqrt{\bar{a}}(1-\bar{e}^2)}{2\bar{e}\sqrt{\mu}} \tag{17c}$$

$$\frac{\partial \dot{\bar{M}}}{\partial \bar{a}}\Big|_{\bar{a},\bar{e},k} = -\frac{3(\bar{a}^2(1+\bar{e}^2)k + 2\bar{e}\mu)}{4\bar{a}^{5/2}\bar{e}\sqrt{\mu}} \tag{18a}$$

$$\frac{\partial \dot{\bar{M}}}{\partial \bar{e}}\Big|_{\bar{a},\bar{e},k} = \frac{3\sqrt{\bar{a}}(1-\bar{e}^2)k}{2\bar{e}^2\sqrt{\mu}} \tag{18b}$$

$$\frac{\partial \dot{\bar{M}}}{\partial k}\Big|_{\bar{a},\bar{e},k} = -\frac{3\sqrt{\bar{a}}(1+\bar{e}^2)}{2\bar{e}\sqrt{\mu}} \tag{18c}$$

Inspecting Eq. (16), in order to match the chief and deputy secular rates to the first-order approximation, the first variations of $\delta\dot{\bar{\omega}}$ and $\delta\dot{\bar{M}}$ must vanish. Therefore, the *first-order necessary conditions for SRP invariant relative orbits* are determined by,

$$\delta\dot{\bar{\omega}} = \frac{\partial \dot{\bar{\omega}}}{\partial \bar{a}}\Big|_{\bar{a},\bar{e},k}\delta\bar{a} + \frac{\partial \dot{\bar{\omega}}}{\partial \bar{e}}\Big|_{\bar{a},\bar{e},k}\delta\bar{e} + \frac{\partial \dot{\bar{\omega}}}{\partial k}\Big|_{\bar{a},\bar{e},k}\delta k = 0 \tag{19a}$$

$$\delta\dot{\bar{M}} = \frac{\partial \dot{\bar{M}}}{\partial \bar{a}}\Big|_{\bar{a},\bar{e},k}\delta\bar{a} + \frac{\partial \dot{\bar{M}}}{\partial \bar{e}}\Big|_{\bar{a},\bar{e},k}\delta\bar{e} + \frac{\partial \dot{\bar{M}}}{\partial k}\Big|_{\bar{a},\bar{e},k}\delta k = 0 \tag{19b}$$

The differential elements $\delta\bar{a}$, $\delta\bar{e}$, and δk are used to determine the deputy's averaged elements using,

$$k_d = k_c + \delta k \tag{20a}$$

$$\bar{a}_d = \bar{a}_c + \delta\bar{a} \tag{20b}$$

$$\bar{e}_d = \bar{e}_c + \delta\bar{e} \tag{20c}$$

As evident in Eq. (19), there are *two constraints* ($\delta\dot{\bar{\omega}} = 0$ and $\delta\dot{\bar{M}} = 0$) that the deputy states must satisfy for a SRP invariant relative motion with respect to a chief solar sail flying in a Sun-synchronous orbit. These two constraints are functions of *three variables* ($\delta\bar{a}$, $\delta\bar{e}$, and δk). Therefore, there is only *one free variable* to choose; once a variable is chosen, the other two free variables are prescribed such that both SRP invariant conditions in Eq. (19) are satisfied. For instance, if the deputy solar sail has a fixed characteristic acceleration, there is only one unique orbit that the deputy can occupy that leads to a SRP invariant relative motion with respect to the chief flying in a Sun-synchronous orbit. The concept of SRP invariant relative orbits are analogous to J_2 invariant relative orbits that were introduced by Alfriend and Schaub in Refs. [20–22]. A *trivial solution* in the families of SRP invariant relative orbits is the leader-follower or string of pearls formation for two solar sails that have the same characteristic acceleration. When two solar sails are in a leader-follower formation ($a_d = a_c$ and $e_d = e_c$) and have the same characteristic acceleration, the secular rates are identically matched, as evident in Eq. (13).

5. Analytical design of SRP invariant relative motion

Given the chief's averaged elements and characteristic acceleration, an SRP invariant formation is established using the procedure in Fig. 3, assuming that the free variable is δk. After choosing a δk value that is within the deputy's reflectivity modulation capability, the two invariant conditions in Eq. (19) are solved for the averaged element differences between the deputy and chief solar sails. The averaged deputy's elements are then determined using Eq. (20). The deputy's osculating elements will then be solved using an iterative process.

A few quasi-periodic relative orbits that are designed using the procedure described are illustrated in Fig. 4. For each case, the formation is propagated for 10 orbits (approximately 55 days). As expected, the first-order SRP invariant relative motion conditions do not provide fully invariant solutions for the nonlinear motion. However, these conditions do achieve almost invariant conditions with only small amounts of drift and distortions apparent in Fig. 4. To illustrate one example numerically, let us assume that two sails have a relative characteristic acceleration of $\delta k = 0.00003 k_c$, then the relative osculating orbital elements $\delta a = -27.088$ [m], $\delta e = 1.0947 \times 10^{-5}$, $\delta\omega = -0.00017453$ [rad], and $\delta M = 0.00017453$ [rad] lead to the relative trajectory shown in Fig. 4(f). Larger δk values lead to faster drift rates since the linear first-order assumption for deriving the necessary conditions is more accurate for smaller δk values. This is evident when comparing the δk values of the relative trajectories in Fig. 4(e) and (f), where δk value used in Fig. 4(e) is approximately an order of magnitude smaller than the δk value used to generate Fig. 4(f).

Note that similar to the Interplanetary Kite-craft Accelerated by Radiation Of the Sun (IKAROS) mission, which was launched by the Japan Aerospace Exploration Agency (JAXA) in 2010, it is assumed that the deputy sail is capable of changing its reflectivity and consequently its characteristic acceleration. The IKAROS mission successfully demonstrated reflectivity modulation technology to control the sail's attitude [23]. To change the surface reflectance, liquid crystal panels on the sail are switched on to produce specular reflection and switched off to create diffuse reflection. With the capability of changing the sail's surface reflectivity, the characteristic acceleration of a sail can be adjusted.

In Section 6, numerical optimization is employed to remove the secular drifts shown in Fig. 4. The numerical approach allows the design of truly SRP invariant solar sail formations in Sun-synchronous orbits.

6. Numerical design of SRP invariant relative motion

The employment of numerical optimization to remove the relative drifts between solar sails has two advantages over the method proposed in Section 5:

- It allows the design variables to be *osculating elements*, thereby side stepping averaged-osculating mapping that can potentially introduce errors into the design of a drift-free formation.
- It allows for the inclusion of other perturbations in the design of a formation. Because of the high altitudes of orbits required to study the geomagnetic tail, it may be necessary to include the third-body effects of the Moon and Sun in the formation design problem.

Note that the third-body effects of the Moon and Sun on the relative motion of a two-craft formation in this orbit regime are shown to be small based on the previous study [11]. Next, the problem formulation is discussed in detail. The formation design problem is then solved numerically using nonlinear programming techniques. MATLAB's constrained nonlinear optimization routine, *fmincon* with *active set* algorithm, is employed to solve the optimization problem. The formation design problem may be summarized as follows. Given the chief's osculating

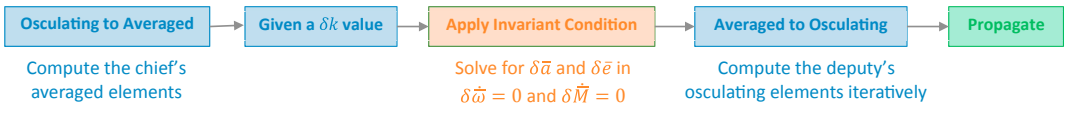

Fig. 3. Procedure to design a SRP invariant solar sail formation in Sun-synchronous orbits.

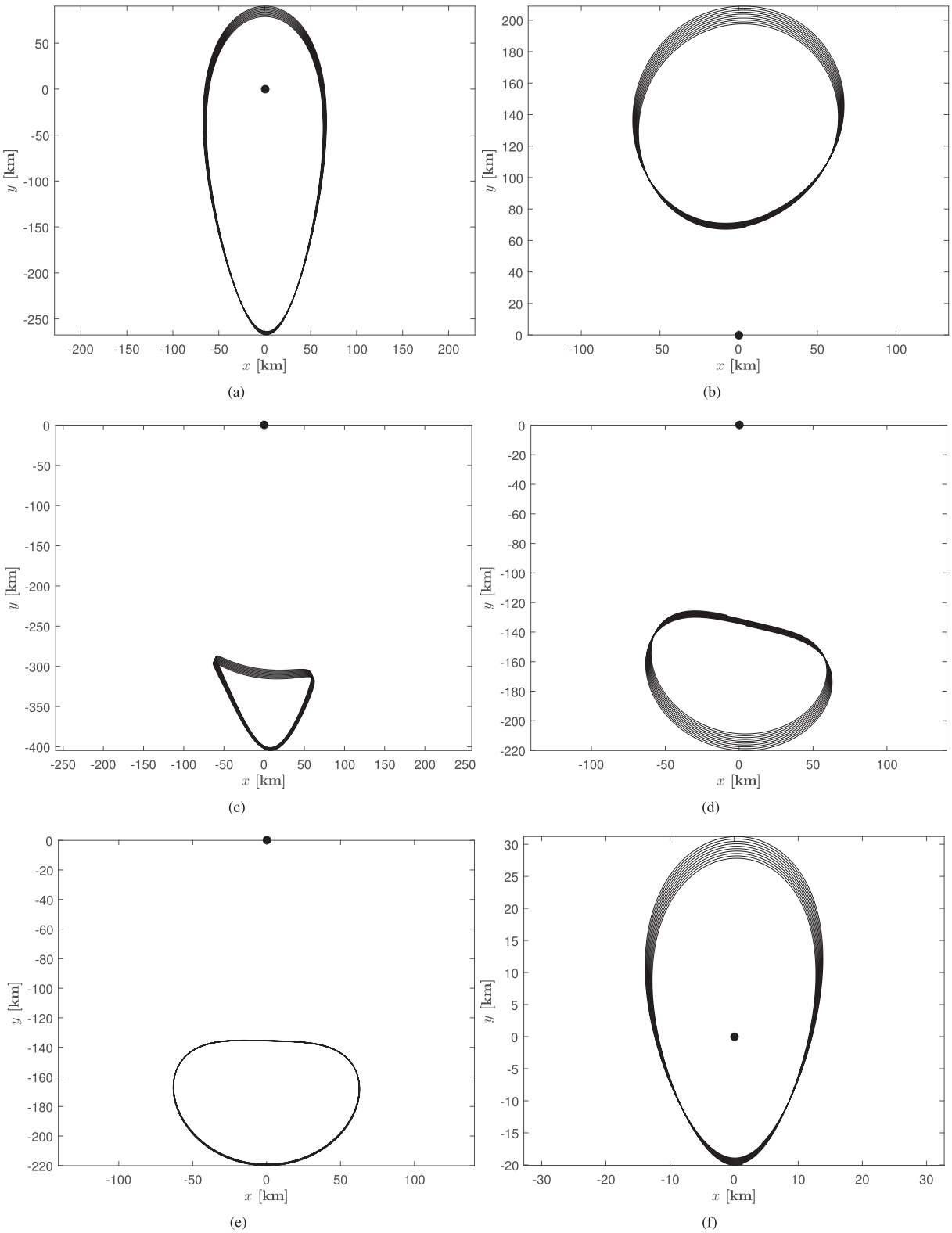

Fig. 4. SRP invariant relative motions designed using first-order analytic conditions expressed in chief's LVLH frame.

elements $\boldsymbol{\alpha}_{c_0} = [\, a_{c_0} \quad e_{c_0} \quad \omega_{c_0} \quad M_{c_0} \,]^T$ at epoch t_0, we must determine the deputy's osculating elements $\boldsymbol{\alpha}_{d_0} = [\, a_{d_0} \quad e_{d_0} \quad \omega_{d_0} \quad M_{d_0} \,]^T$ at epoch t_0 such that the relative motion is SRP invariant. Let l denote the sail's mean longitude, defined as,

$$l = \omega + M \tag{21}$$

The total relative change in mean longitude over an arbitrary number of complete revolutions is defined as,

$$\Delta l = \int_{t_0}^{t_f} \left(\dot{l}_d(t) - \dot{l}_c(t) \right) \mathrm{d}t \tag{22}$$

The variable Δl indicates how much the deputy has drifted apart with respect to the chief over a given time span. Given the chief's osculating

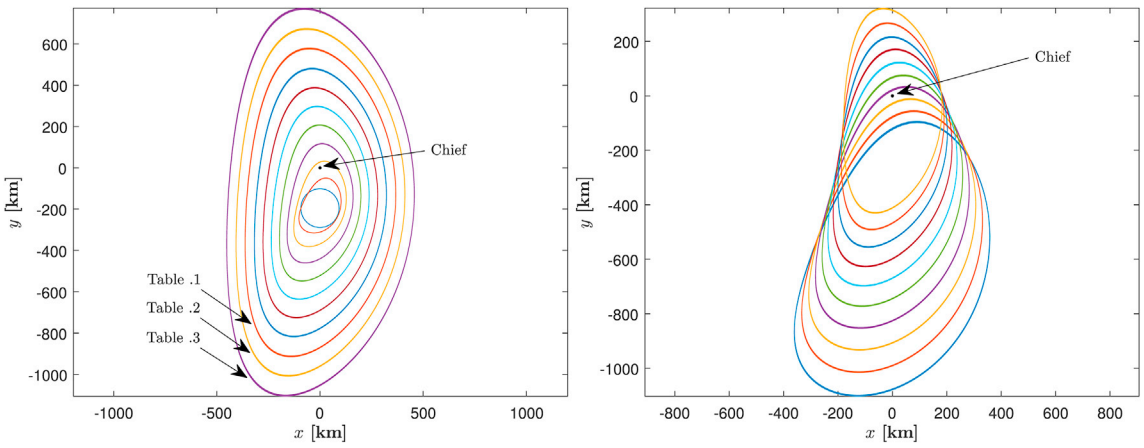

(a) Varying a_{d_0} while keeping M_{d_0} constant (b) Varying M_{d_0} while keeping a_{d_0} constant

Fig. 5. Families of truly SRP invariant relative orbits expressed in chief's LVLH frame.

elements $\boldsymbol{\alpha e}_{c_0}$, a two-craft formation design algorithm is proposed as follows,

$$\begin{aligned} &\text{minimize} && J = |\Delta l| \\ &\text{with respect to} && a_{d_0}, e_{d_0} \\ &\text{subject to} && \ddot{\boldsymbol{r}}_c = -\frac{\mu}{r_c^3}\boldsymbol{r}_c + \boldsymbol{a}_{s_c} \\ & && \ddot{\boldsymbol{r}}_d = -\frac{\mu}{r_d^3}\boldsymbol{r}_d + \boldsymbol{a}_{s_d} \\ &\text{free variables} && k_d, M_{d_0}, \omega_{d_0} \end{aligned} \tag{23}$$

In this formulation, it is assumed that the free variable is the deputy's characteristic acceleration k_d while the a_{d_0} and e_{d_0} osculating elements are left to be determined numerically, such that the relative motion is SRP invariant. The algorithm allows for the minimization of the relative drift between the two sails through a search of the osculating element space. The minimization of total relative change in mean longitude over a specific time span is equivalent to matching the average longitude rates. The first-order SRP invariant relative motion conditions using osculating elements are used to provide an initial guess for the deputy's elements, since nonlinear programming problems require an initial guess to solve the problem. These first-order conditions provide a very good initial starting point for the nonlinear optimizer to converge onto a truly invariant relative motion solution. With general initial conditions, the optimizer did not always converge to an invariant relative motion. The problem formulation in Eq. (23) can be modified to have either the semi-major axis or eccentricity as a free variable rather than the characteristic acceleration. Hence, the formulation may be equivalently rewritten as

$$\begin{aligned} &\text{minimize} && J = |\Delta l| \\ &\text{with respect to} && e_{d_0}, k_d \\ &\text{subject to} && \ddot{\boldsymbol{r}}_c = -\frac{\mu}{r_c^3}\boldsymbol{r}_c + \boldsymbol{a}_{s_c} \\ & && \ddot{\boldsymbol{r}}_d = -\frac{\mu}{r_d^3}\boldsymbol{r}_d + \boldsymbol{a}_{s_d} \\ &\text{free variables} && a_{d_0}, M_{d_0}, \omega_{d_0} \end{aligned} \tag{24}$$

In Eq. (24), the free variable is chosen to be the deputy's semi-major axis a_{d_0} while the algorithm searches for the corresponding e_{d_0} and k_d that leads to an SRP invariant relative motion. The deputy's mean anomaly M_{d_0} and ω_{d_0} are the other free variables that can be tweaked to control the differential elements δM and $\delta\omega$ for designing formation geometries of different size and shape. Although ω_{d_0} is a free variable, there are lower and upper bounds for how much ω_{d_0} can change with respect to the Sun's longitude angle λ_s. This is due to the Sun-synchronous condition that each sail must satisfy. Therefore, the deputy's ω_{d_0} must remain close to the Sun's longitude angle λ_s.

An example of the algorithm proposed in Eq. (24) is illustrated in Fig. 5. A family of truly SRP invariant relative orbits are illustrated in Fig. 5(a). In these examples, the deputy's semi-major axis is varied such that $0 \leqslant \delta a_0 \leqslant 1$ km, while keeping δM_0 constant. In Fig. 5(b), the δM_0 is varied while keeping δa_0 constant. For both simulations, it is assumed that $\delta\omega_0 = 0$ $(\omega_{d_0} = \omega_{c_0} = \lambda_{s_0})$. Each trajectory is propagated for 10 orbits. As evident in both Fig. 5(a) and (b), the relative motion does not experience any relative drift, unlike the secular drifts that arise in Fig. 4 due to the first-order approximation of the SRP invariant relative orbit conditions. The optimized initial conditions for a few of the SRP invariant relative orbits illustrated in Fig. 5(a) are tabulated in Tables 1–3, corresponding to the three largest formations, respectively.

Table 1
Optimized initial conditions for SRP invariant relative motions shown in Fig. 5(a).

Parameters	Chief	Deputy	Unit
a	131874.57700657	131875.27700657	km
e	0.46798169	0.46566884	
ω	0°	0°	degree
M	180°	179.92684586°	degree
k	0.12220198	0.12142995	mm/s^2

Table 2
Optimized initial conditions for SRP invariant relative motions shown in Fig. 5(a).

Parameters	Chief	Deputy	Unit
a	131874.57700657	131875.37700657	km
e	0.46798169	0.46531466	
ω	0°	0°	degree
M	180°	179.92684586°	degree
k	0.12220198	0.12131202	mm/s^2

Table 3
Optimized initial conditions for SRP invariant relative motions shown in Fig. 5(a).

Parameters	Chief	Deputy	Unit
a	131874.57700657	131875.47700657	km
e	0.46798169	0.46497128	
ω	0°	0°	degree
M	180°	179.92684586°	degree
k	0.12220198	0.12119774	mm/s^2

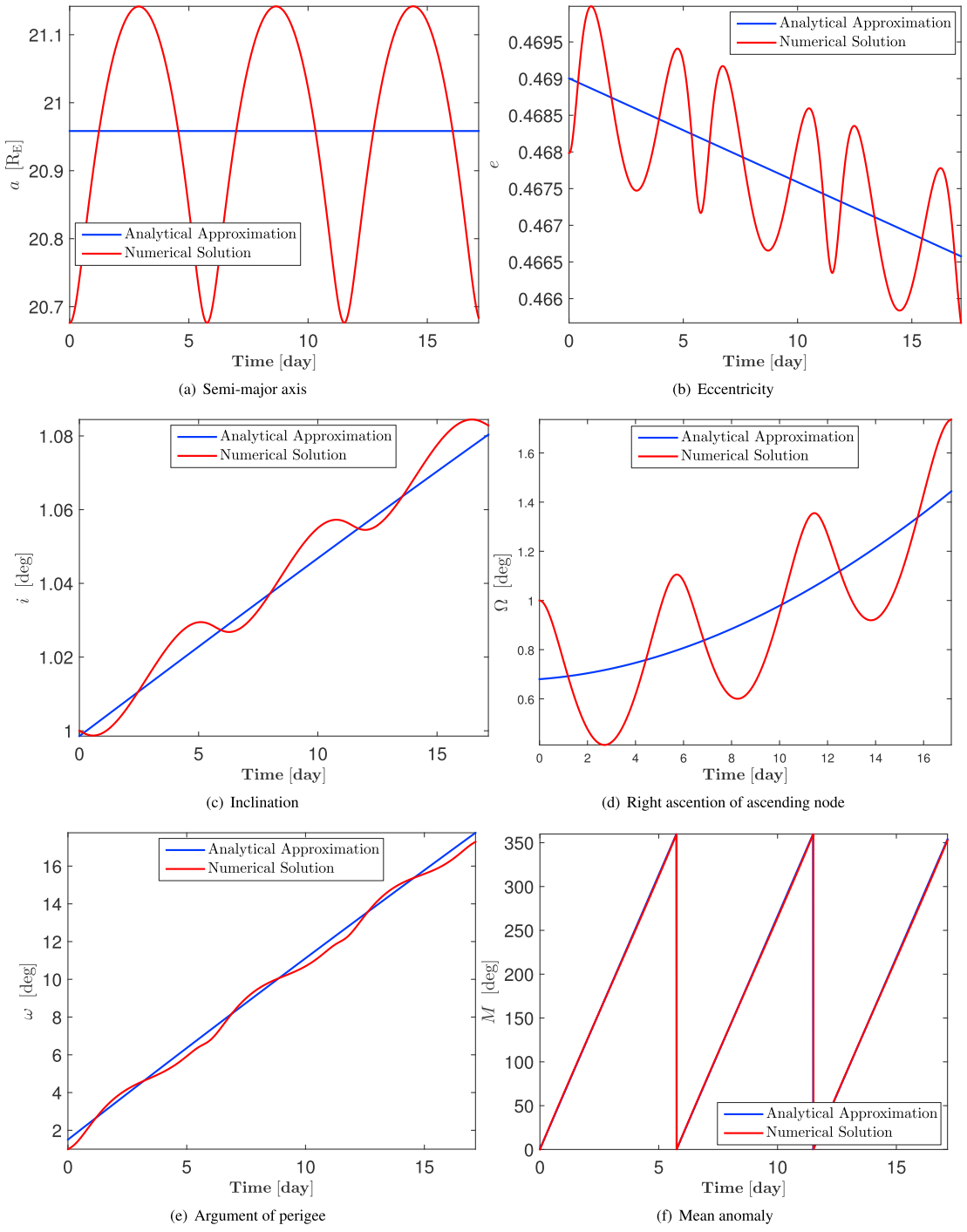

(a) Semi-major axis (b) Eccentricity

(c) Inclination (d) Right ascention of ascending node

(e) Argument of perigee (f) Mean anomaly

Fig. 6. Verification of averaged orbital element rates resulting from changes in the nominal Sun-pointing attitude.

7. Effects of uncertainty in attitude

Averaging theory is applied to determine the secular drifts in terms of the presence of a constant attitude error. This is mainly motivated by the fact that the solar sails are assumed to maintain a Sun-pointing attitude at all times for the purpose of precessing their orbit apse lines Sun-synchronously. Assuming that the sail's normal vector has an attitude error with respect to the nominal Sun-pointing attitude described by the two constant angles $\delta\alpha$ and $\delta\phi$, we have,

$$\phi = \phi_{\text{nominal}} + \delta\phi = \pi - f + \delta\phi \tag{25a}$$

$$\alpha = \alpha_{\text{nominal}} + \delta\alpha = \delta\alpha \tag{25b}$$

After substituting the new ϕ and α into Eq. (2) and substituting the result into the Gauss variational equations, the osculating orbital elements are averaged with respect to mean anomaly in order to remove the short-period variations,

$$\dot{\bar{a}} = \frac{1}{2\pi}\int_0^{2\pi} \dot{a}\, \mathrm{d}M \tag{26a}$$

$$\dot{\bar{e}} = \frac{1}{2\pi}\int_0^{2\pi} \dot{e}\, \mathrm{d}M \tag{26b}$$

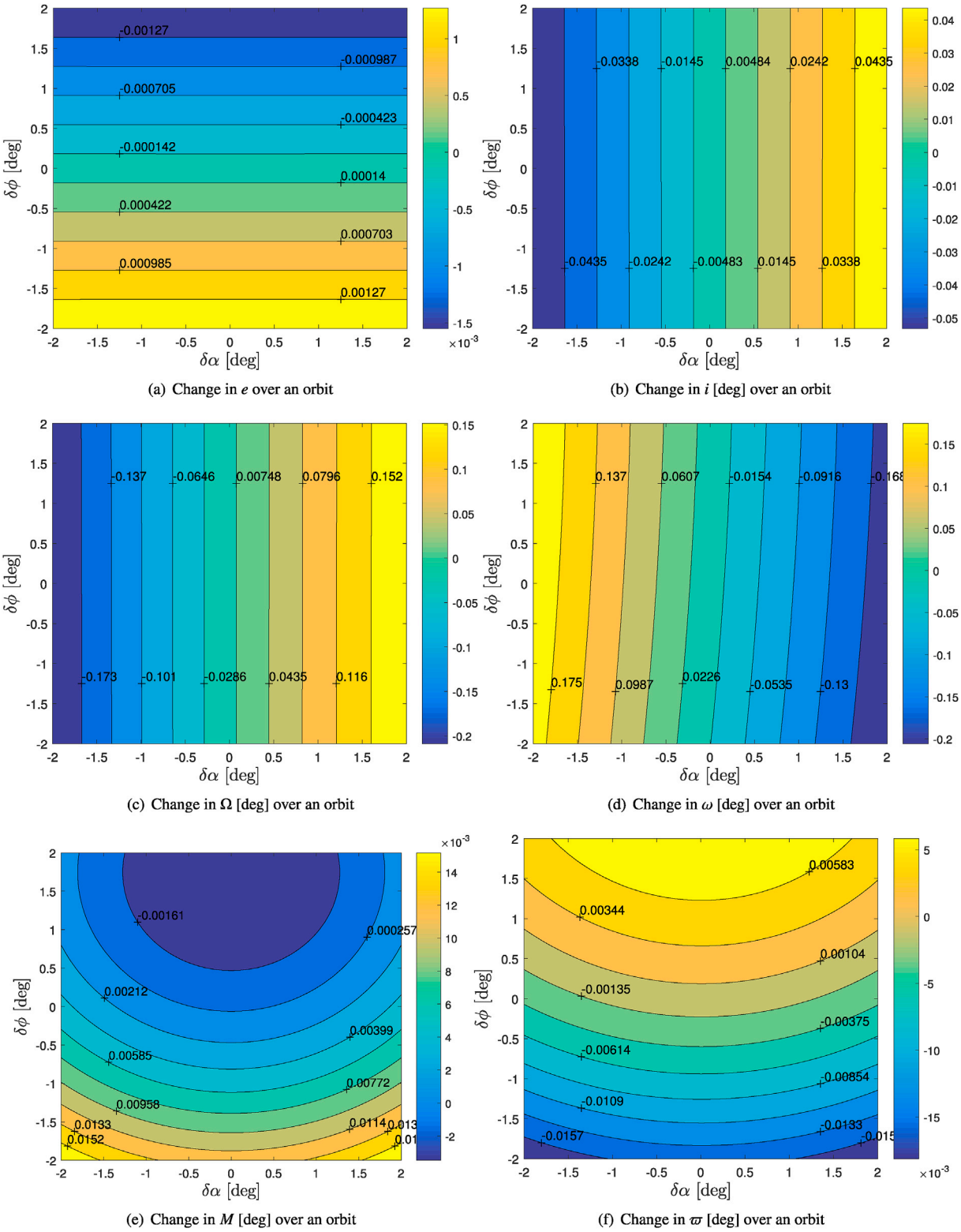

(a) Change in e over an orbit

(b) Change in i [deg] over an orbit

(c) Change in Ω [deg] over an orbit

(d) Change in ω [deg] over an orbit

(e) Change in M [deg] over an orbit

(f) Change in ϖ [deg] over an orbit

Fig. 7. Sensitivity of orbital elements to constant attitude error.

$$\dot{\bar{i}} = \frac{1}{2\pi}\int_0^{2\pi} \dot{i}\, \mathrm{d}M \tag{26c}$$

$$\dot{\bar{\Omega}} = \frac{1}{2\pi}\int_0^{2\pi} \dot{\Omega}\, \mathrm{d}M \tag{26d}$$

$$\dot{\bar{\omega}} = \frac{1}{2\pi}\int_0^{2\pi} \dot{\omega}\, \mathrm{d}M \tag{26e}$$

$$\dot{\bar{M}} = \frac{1}{2\pi}\int_0^{2\pi} \dot{M}\, \mathrm{d}M \tag{26f}$$

Upon taking the integration and simplification, the average orbital

element rates for a solar sail in Sun-synchronous orbits with a constant attitude error are determined to be,

$$\dot{\bar{a}} = 0 \tag{27a}$$

$$\dot{\bar{e}} = -\frac{3k\sqrt{\bar{a}(1-\bar{e}^2)}}{2\sqrt{\mu}}\cos\delta\alpha\sin\delta\phi \tag{27b}$$

$$\dot{\bar{i}} = \frac{3\bar{e}k\cos\bar{\omega}}{2\sqrt{\frac{\mu\left(1-\bar{e}^2\right)}{\bar{a}}}}\sin\delta\alpha \tag{27c}$$

$$\dot{\bar{\Omega}} = \frac{3\bar{e}k\csc\bar{i}\sin\bar{\omega}}{2\sqrt{\frac{\mu\left(1-\bar{e}^2\right)}{\bar{a}}}}\sin\delta\alpha \tag{27d}$$

$$\dot{\bar{\omega}} = \frac{3k\sqrt{\bar{a}(1-\bar{e}^2)}}{2\bar{e}\sqrt{\mu}}\cos\delta\alpha\cos\delta\phi - \frac{3\bar{e}k\cot\bar{i}\sin\bar{\omega}}{2\sqrt{\frac{\mu\left(1-\bar{e}^2\right)}{\bar{a}}}}\sin\delta\alpha \tag{27e}$$

$$\dot{\bar{M}} = \bar{n} - \frac{3\bar{a}^2(1+\bar{e}^2)k}{2\bar{a}^{3/2}\bar{e}\sqrt{\mu}}\cos\delta\alpha\cos\delta\phi \tag{27f}$$

The main advantage of deriving the average orbital element rates is their elegant simplified form, which immediately reveals a great deal about the long-term dynamics of the system. Additionally, they are more computationally efficient than the full osculating equations of motion. To verify the validity of Eq. (27), these approximate analytic expressions are compared to the full osculating Gauss variational equations in Eq. (9) for $(\delta\phi,\ \delta\alpha) = (1^\circ,\ 1^\circ)$. As illustrated in Fig. 6, the averaged equations correctly predict the secular growth in the orbital elements resulting from the errors in the sail's Sun-pointing attitude.

Next, the averaged rates for the orbital elements in Eq. (27) are used to generate the contour plots in Fig. 7. These plots illustrate the net change in the orbital elements over an orbit due to constant errors in the sail's orientation. The net change in eccentricity over an orbit is shown in Fig. 7(a). As expected from Eq. (27b), the effects of the $\delta\phi$ attitude errors are dominated over the span of small $\delta\alpha$ values. Even for very small $\delta\phi$ values, the eccentricity experiences a change of approximately 0.0001. The net change in the orbit inclination is shown in Fig. 7(b). The variation in inclination is completely dominant by the out-of-plane variation in the sail's attitude $\delta\alpha$. Errors in the ϕ angle will only affect the inclination for substantially high $\delta\phi$ values. These effects creep in through the variations in the e and ω orbital elements as evident by Eq. (27c). Similar to inclination, Fig. 7(c) shows that the effects of out-of-plane angle $\delta\alpha$ are dominant over the in-plane angle $\delta\phi$ in changing the right ascension of the ascending node. As expected, the argument of perigee is affected more by the in-plane variation relative to the right ascension of the ascending node. Fig. 7(f) illustrates the net change in the longitude of orbit's perigee ($\varpi = \omega + \Omega$). Based on these figures, one can conclude

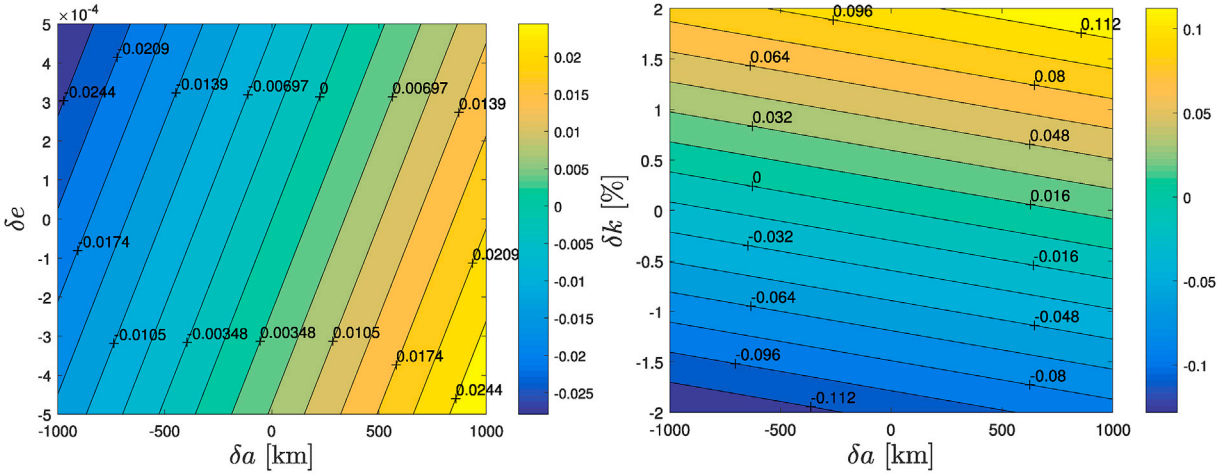

(a) Change in ω [deg] over one orbit due to errors in a & e

(b) Change in ω [deg] over one orbit due to errors in a & k

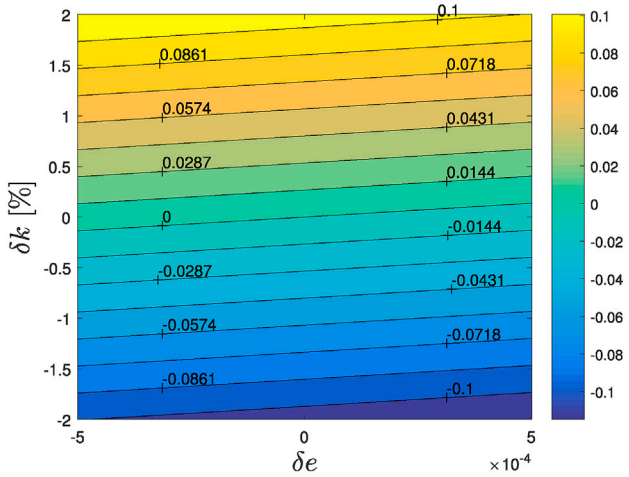

(c) Change in ω [deg] over one orbit due to errors in e & k

Fig. 8. Sensitivity of argument of perigee to errors in semi-major axis, eccentricity, and the sail's characteristic acceleration (reflectivity).

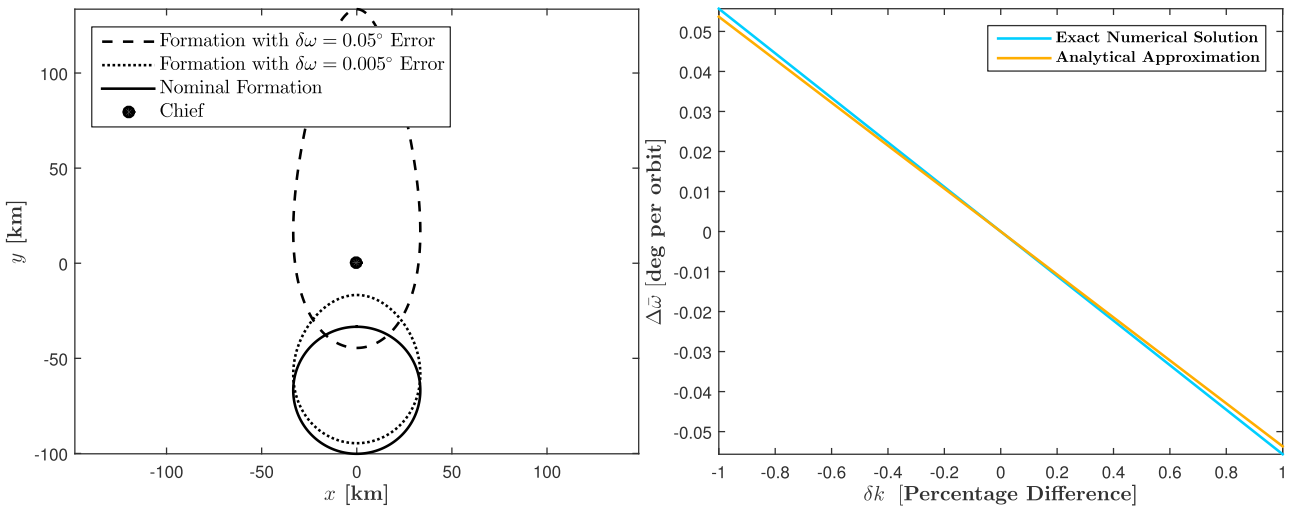

(a) Relative motion in chief's LVLH frame

(b) Change in ω [deg] over one orbit due to errors in k

Fig. 9. Effects of $\delta\omega$ error on leader-follower formation.

that, uncorrected attitude errors can quickly lead to the divergence of the nominal orbit or cause secular growth in the relative geometry between two solar sails.

8. Effects of uncertainty in elements and reflectivity

In this section, we evaluate the effects of errors in the orbital elements and reflectivity on the Sun-synchronous condition, which requires $\omega = \lambda_s$. The metric chosen is how much change ω experiences over an orbit given uncertainty in other orbital elements and reflectivity. To do this, the first variation of the rate of change in the argument of perigee $\delta\dot{\bar{\omega}}(a, e, k)$, given in Eq. (19a), is used to determine the net change in argument of perigee over one orbit using $\Delta\bar{\omega} = T \times \delta\dot{\bar{\omega}}$, where T is the orbit period.

The contour plot shown in Fig. 8(a) illustrates the effects of uncertainty in the semi-major axis and eccentricity on the argument of perigee. The effects of unmodeled errors in characteristic acceleration and uncertainty in semi-major axis are shown in Fig. 8(b). Fig. 8(c) illustrates the change in argument of perigee due to errors in eccentricity and characteristic acceleration. As evident, the combined effects of uncertainties in eccentricity and characteristic acceleration can lead to changes in the argument of perigee as large as 0.1° over an orbit. Depending on the objective of the mission, this difference in argument of perigee may not be tolerable for the relative motion, especially for missions such as Magnetosphere Multi-Scale (MMS), where the spacecraft are expected to maintain a tight formation of a certain size and shape. MMS mission requires four spacecraft to form a regular tetrahedron of a particular size around the orbit apogee [24,25]. The tetrahedron formation must change its size, ranging from 400 km to 7 km in terms of averaged side length. Fig. 9(a) illustrates the effects of uncertainty in the differential elements, namely the argument of perigee, on the relative motion geometry. As evident in the figure, an uncertainty in the argument of perigee of the size $\delta\omega = 0.05^\circ$ significantly changes the shape of the nominal leader-follower formation, leading to about a 100 km error in the along-track (y) direction. Using Fig. 9(b), one can conclude that an uncertainty in reflectivity larger than 0.1% leads to significant changes in the size and shape of the formation, which may not satisfy the requirements for tight formations such as the one being flown in the MMS mission.

9. Conclusion

In this paper, the effects of SRP perturbations in Sun-synchronous orbits are studied in detail using the averaging theory, which leads to the identification of the secular variations in the orbital elements. Next, the analytic first-order necessary conditions for a SRP invariant relative motion are derived, assuming that all solar sails in the formation maintain a Sun-pointing attitude. Numerical simulations are used to verify the validity of the conditions derived. It is shown that the first-order necessary conditions lead to a quasi-periodic formation, as opposed to truly SRP invariant relative motion. This is a direct result of the first-order linear approximation used to derive the necessary conditions. Next, the problem of formation design is explored in detail using numerical optimization for the two-craft formations. It is shown how the slow secular drifts resulting from the analytic first-order conditions can be removed using numerical techniques. This leads to the design of truly SRP invariant solar sail formations. Next, the average effects of small constant inaccuracies in the Sun-pointing attitude on the average rates of orbital elements are derived analytically. The sensitivity analysis with respect to the sail's characteristic acceleration is investigated and it is shown that larger than 0.1% uncertainty in the characteristic acceleration of a sail leads to a significant changes in the size and the shape of a tight formation.

Acknowledgments

The authors are thankful for Dr. Daniel Scheeres's technical input and invaluable guidance provided for this paper, especially on the use of averaging theory for determining the long-term effects of the SRP force.

References

[1] S. Curtis, The Magnetospheric Multiscale Mission… Resolving Fundamental Processes in Space Plasmas, NASA Goddard Space Flight Center NASA/TM2000-209883, 1999.
[2] G. Prölss, Physics of the Earths Space Environment: an Introduction, Springer Science & Business Media, 2012.
[3] C.R. McInnes, M. MacDonald, V. Angelopolous, D. Alexander, Geosail: exploring the geomagnetic tail using a small solar sail, J. Spacecr. Rocket. 38 (4) (2001) 622–629.
[4] M. Macdonald, G. Hughes, C. McInnes, A. Lyngvi, P. Falkner, A. Atzei, Geosail: an elegant solar sail demonstration mission, J. Spacecr. Rocket. 44 (4) (2007) 784–796.
[5] M. Macdonald, C. McInnes, Analytical control laws for planet-centered solar sailing, J. Guid. Control, Dyn. 28 (5) (2005) 1038–1048.
[6] S. Gong, G. Yunfeng, J. Li, Solar sail formation flying on an inclined earth orbit, Acta Astronaut. 68 (1) (2011) 226–239.
[7] J. Mu, S. Gong, J. Li, Reflectivity-controlled solar sail formation flying for magnetosphere mission, Aerosp. Sci. Technol. 30 (1) (2013) 339–348.
[8] J. Mu, S. Gong, J. Li, Coupled control of reflectivity modulated solar sail for geosail formation flying, J. Guid. Control, Dyn. (2014) 1–12.
[9] J. Mu, S. Gong, P. Ma, J. Li, Dynamics and control of flexible spinning solar sails under reflectivity modulation, Adv. Space Res. 56 (8) (2015) 1737–1751.

[10] T. Hu, S. Gong, J. Mu, J. Li, T. Wang, W. Qian, Switch programming of reflectivity control devices for the coupled dynamics of a solar sail, Adv. Space Res. 57 (5) (2016) 1147–1158.
[11] K. Parsay, H. Schaub, Designing solar sail formations in sun-synchronous orbits for geomagnetic tail exploration, Acta Astronaut. 107 (2015) 218–233.
[12] C.R. McInnes, Solar Sailing: Technology, Dynamics and Mission Applications, Springer, 2004.
[13] K. Alfriend, S.R. Vadali, P. Gurfil, J. How, L. Breger, Spacecraft Formation Flying: Dynamics, Control and Navigation, vol. 2, Butterworth-Heinemann, 2009.
[14] A.J. Rosengren, D.J. Scheeres, On the milankovitch orbital elements for perturbed keplerian motion, Celest. Mech. Dyn. Astron. 118 (3) (2014) 197–220.
[15] D. Scheeres, A. Rosengren, J. Mcmahon, The dynamics of high area-to-mass ratio objects in earth orbit: the effect of solar radiation pressure, Spacefl. Mech. 140.
[16] A.J. Rosengren, D.J. Scheeres, Long-term dynamics of high area-to-mass ratio objects in high-earth orbit, Adv. Space Res. 52 (8) (2013) 1545–1560.
[17] D. Scheeres, Satellite Dynamics about Small Bodies, Averaged solar radiation pressure effects1, Ann Arbor 1001, 1999, pp. 48109–52140.
[18] D. Scheeres, F. Marzari, L. Tomasella, V. Vanzani, Rosetta mission: satellite orbits around a cometary nucleus, Planet. Space Sci. 46 (6) (1998) 649–671.
[19] R.H. Battin, An Introduction to the Mathematics and Methods of Astrodynamics, revised Edition, AIAA Education Series, 1999.
[20] H. Schaub, S.R. Vadali, J.L. Junkins, K.T. Alfriend, Spacecraft formation flying control using mean orbit elements, J. Astronaut. Sci. 48 (1) (2000) 69–87.
[21] H. Schaub, K.T. Alfriend, J2 invariant relative orbits for spacecraft formations, Celest. Mech. Dyn. Astron. 79 (2) (2001) 77–95.
[22] H. Schaub, Incorporating secular drifts into the orbit element difference description of relative orbits, Adv. Astronaut. Sci. 114 (2003) 239–257.
[23] O. Mori, Y. Shirasawa, Y. Mimasu, Y. Tsuda, H. Sawada, T. Saiki, T. Yamamoto, K. Yonekura, H. Hoshino, J. Kawaguchi, et al., Overview of ikaros mission, in: Advances in Solar Sailing, Springer, 2014, pp. 25–43.
[24] S.P. Hughes, General method for optimal guidance of spacecraft formations, J. Guid. control, Dyn. 31 (2) (2008) 414–423.
[25] S.P. Hughes, Formation design and sensitivity analysis for the magnetospheric multiscale mission (mms), in: AIAA/AAS Astrodynamics Specialist Conference, Honolulu, HI, 2008.